IEEE Journal of Translational Engineering in Health and Medicine

Received 6 April 2023; revised 21 June 2023; accepted 7 July 2023.
Date of publication 17 July 2023; date of current version 8 August 2023.

Digital Object Identifier 10.1109/JTEHM.2023.3295775

Breathing-Associated Facial Region Segmentation for Thermal Camera-Based Indirect Breathing Monitoring

JUNHWAN KWON[1], OYUN KWON[1], KYEONG TAEK OH[1], JEONGMIN KIM[2], AND SUN K. YOO[1]

[1]Department of Medical Engineering, Yonsei University College of Medicine, Seoul 03722, South Korea
[2]Department of Anesthesiology and Pain Medicine, Severance Hospital, College of Medicine, Seoul 03722, South Korea

CORRESPONDING AUTHORS: S. K. YOO (sunkyoo@yuhs.ac) AND J. KIM (anesjeongmin@yuhs.ac)

This work was supported in part by the Korea Medical Device Development Fund grant funded by the Korean Government under Project HW20C2151; and in part by the Industrial Technology Innovation Program (Development of Emotional Cognitive and Sympathetic Artificial Intelligence (AI) Service Technology for Remote (Non-Face-to-Face) Learning and Industrial Sites) funded by the Ministry of Trade, Industry and Energy (MOTIE, South Korea) under Grant 20012603.

This work involved human subjects or animals in its research. Approval of all ethical and experimental procedures and protocols was granted by Severance Hospital under Reference No. 4-2020-1320.

ABSTRACT Breathing can be measured in a non-contact method using a thermal camera. The objective of this study investigates non-contact breathing measurements using thermal cameras, which have previously been limited to measuring the nostril only from the front where it is clearly visible. The previous method is challenging to use for other angles and frontal views, where the nostril is not well-represented. In this paper, we defined a new region called the breathing-associated-facial-region (BAFR) that reflects the physiological characteristics of breathing, and extract breathing signals from views of 45 and 90 degrees, including the frontal view where the nostril is not clearly visible. Experiments were conducted on fifteen healthy subjects in different views, including frontal with and without nostril, 45-degree, and 90-degree views. A thermal camera (A655sc model, FLIR systems) was used for non-contact measurement, and biopac (MP150, Biopac-systems-Inc) was used as a chest breathing reference. The results showed that the proposed algorithm could extract stable breathing signals at various angles and views, achieving an average breathing cycle accuracy of 90.9% when applied compared to 65.6% without proposed algorithm. The average correlation value increases from 0.587 to 0.885. The proposed algorithm can be monitored in a variety of environments and extract the BAFR at diverse angles and views.

INDEX TERMS Breathing, thermal camera, physiological features, noncontact, Markov random field. (Clinical Impact)The proposed algorithm shows the feasibility of non-contact breathing reliable monitoring that versatile and accurate than previous methods. The proposed algorithm could be used to monitor breathing in various clinical environments, including isolated wards, operation rooms, and intensive care units with high infection risks.

I. INTRODUCTION

Breathing reflects the human physiological state, and breathing signals provide valuable vital information that is sensitive to clinical conditions [1], [2], [3], [4]. Breathing provides clinical information about cardiac arrest, emotional stress, cognitive loads, and severe pneumonia [5], [6], [7], [8]. It is important to reliably monitor breathing signals. Breathing signals are generally measured using contact methods (e.g., respiration belts [9], spirometers [10], [11], capnography [12], [13], and thoracic impedance tomography (TIG) [14], [15]). However, contact methods are inconvenient and increase infection risks. In particular, TIG interferes with body impedance during some measurements, such as electrosurgical units (ESUs) and movements. Another way to measure breathing is the noncontact method. Technological advances have made it possible to measure breathing

signals with noncontact methods (e.g., Wi-Fi Sensing [16], RGB cameras [17], [18], [19], Microphones [20], Doppler radar [21], [22], depth cameras [23], [24], and thermal cameras [25], [26], [27], [28], [29], [30], [31], [32], [33], [34]). These methods including thermal cameras avoid the disadvantages of the contact method but are limited by the difficulty of reliably measuring breaths. In particular, thermal camera has the advantage of being able to measure in darkness and scalability to measure physiological information related to the temperature.

In order to measure reliable breathing non-contact, the breathing-associated region should be well-defined. RGB cameras obtain the visible light area around an object, and depth cameras obtain the depth information of an object; both cameras generate two-dimensional information based on light rays reflected by the object's structure. Therefore, these cameras can provide highly accurate structural information. However, thermal cameras do not directly measure structural information and instead indirectly measure the radiation generated by the structure, which results in a relative loss of structural information. Breathing-Associated Facial Region (BAFR) segmentation using structural methods has limited performance due to the characteristics of these thermal cameras.

In previous studies, breathing signals were estimated according to temperature changes in the nostril region. The Region of Interest (ROI) is defined by measuring the temperature changes around the nostril using anatomical properties. Fei and Pavlidis [27] proposed a measurement region of interest (MROI) using the shape property of the nasal tissue. The MROI was defined to calculate the horizontal and vertical projection profiles of the nasal tissue. The projection profiles were obtained by averaging the row and column pixel values. With this method, the position of the gradient changes if the angle of the nose in the camera view is not perpendicular. Thus, the angle data must be preprocessed to identify the intended nostril position. Moreover, Basu et al. [36] proposed a semiautomatic method in which the ROI was selected as a circular region around the nose by identifying the coldest point on the face and manually tuning the region. Alkali et al. [37] proposed a method of localizing the nose using gradients across the face; this method determines the position of the nose by dividing the facial position with the largest gradient by the point on the x and y-axes. Maurya et al. [38] extracted the location coordination of the nose based on RGB camera data by simultaneously acquiring information with RGB and thermal cameras. Although this method may be more accurate in distinguishing structures than the use of a thermal camera alone, it is limited by its high cost. And the inclusion of the nostril region had an important effect on the ability of the method to structurally find BAFRs using thermal cameras because of significant breathing and temperature changes in the nostril area in the thermal face data. However, structural methods cannot be used when the thermal face is obtained from a view that excludes the nostril area. Additionally, even if the nostril region is included, the size and shape of the nostril vary considerably between individuals, and the location is specified according to a rule-based structural method. As a result, these methods using structural information cannot obtain accurate BAFRs in thermal face data. Furthermore, large errors may occur depending on the angle or view of the nose when the temperature gradient of the thermal face structure is used. When breathing signals are extracted at various angles and views, more BAFRs that are unassociated with breathing are included than when breathing signals are extracted from the front view. The BAFRs and the nostril are obscured and observed asymmetrically depending on the view. BAFRs are important for obtaining an accurate breathing rate; the breathing cycle cannot be detected because the temperature change in the nose region due to breathing is insignificant.

In this study, we propose a method based on the physiological feature that temperature changes with breathing and that the physiological features of breathing are expressed as temperature changes in thermal camera data. Temperature changes due to breathing occur not only in the nostril area, where the breathing-associated effects are greatest, but also in other regions that are affected by air flow. The proposed algorithm extracts the breathing-associated probability map and labels the pixels into breathing-associated and non-breathing regions using Markov Random Fields (MRFs). The breathing-associated probability map is calculated using the temperature difference due to breathing and periodical features of the breathing waveform. The proposed algorithm is not designed to identify the location of the nostril hole but to label the regions displaying temperature changes due to breathing in pixels, regardless of the angle or thermal camera view. This proposed segmentation algorithm can extract breathing-associated regions near the nose region according to thermal camera data, regardless of the nose angle. The proposed segmentation algorithm can extract reliable breathing signals to calculate the accurate breathing rate in various clinical environments such as isolated wards, ICUs, and operation rooms etc.

In addition, the proposed algorithm does not simply define the BAFR as the nostril hole but visualizes the actual BAFR due to breathing. The visualization of the BAFRs has the potential insight to be utilized as a method to monitor breathing. We acquired thermal face data during breathing at various angles and camera views and simultaneously extracted breathing signals with a chest belt sensor as a reference. The camera views used in the experiment included the front, 45 degrees, and 90 degrees. In the frontal view, thermal face data with and without the nostril hole were acquired. A segmentation mask was extracted by applying the proposed algorithm to each set of acquired data. Additionally, the breathing signals were extracted with and without the application of a segmentation mask. Each extracted breathing signal was compared to the reference obtained with the chest belt sensor.

IEEE Journal of Translational Engineering in Health and Medicine

The main contributions of this paper are summarized as follows:

1) The proposed algorithm defines a Breathing Associated Facial Region (BAFR) which reflects the physiological features of breathing in thermal camera.
2) The proposed algorithm extracts reliable breathing signals from views of 45 and 90 degrees, including the frontal view where the nostril is not clearly visible.
3) The proposed algorithm has a potential clinical impact, as it could be used to stable monitor breathing in various clinical environments, including high-risk areas.

II. METHODOLOGY

We applied pixel-clustering algorithm for breathing-associated segmentation using a thermal camera. Segmentation tasks can be modeled by MRFs. MRFs have been used in many segmentation applications [39], [40], [41], [42]. The proposed MRF segmentation approach aims to estimate the breathing-associated pixel labels with respect to the physiological breathing features. The flow of air due to breathing occurs through the nostril passages. However, not only does the shape, and size of each individual's nostril vary, but the range of pixel regions affected by the thermal energy gradient is represented in an arbitrary form. This study uses MRF segmentation based on a pixel-clustering method to consider the unstructured local dependence. MRF segmentation is suited for pixel-wise clustering of breathing-associated temperature gradients. A key component of the MRF model is the energy, defined as the sum of the feature field's energy and the label field's energy. In our approach, the feature field corresponds to breathing-associated features, while the label field comprises two classes: breathing-associated and non-associated regions. The energy of the feature field provides a measure of how well the breathing-associated probability feature values of the pixels fit the segmentation model, whereas the energy of the label field gauges how well the pixel labels correspond to the local dependence of thermal changes associated with breathing. This segmentation estimation is formulated as a maximum a posteriori (MAP) estimation using the iterated conditional modes (ICM) approach, which is a greedy algorithm that iteratively updates the breathing-associated pixel labels of the MRF nodes. During each iteration, the MRF node is allowed to change its label; the updates are applied to all nodes until the algorithm reaches convergence. In this study, the ICM algorithm is iterated for 30 epochs. As this MRF method is sensitive to initialization, we estimated a prior map of breathing-associated features. An initialization was created for each frame based on the middle probability in the prior map.

A. RELATIONSHIP BETWEEN BREATHING AND THERMAL CHANGES

To define the breathing-associated pixels, it is necessary to know the physiological characteristics of breathing and how these characteristics are expressed in thermal camera data.

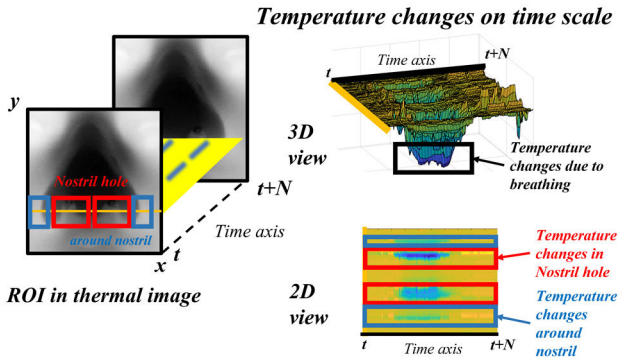

FIGURE 1. Relationship between breathing and thermal changes at around nostril holes.

Breathing is a periodic outflow of internal lung air and inflow of external air. The periodical features vary depending on the breathing cycle, but inhalation and exhalation are generally present. Thermal cameras can be used to observe temperature changes during the breathing cycle [43], [44], [45], [46] at nostril holes. In addition, breathing airflow is greatest at the nostril holes, but there are other regions around the nostril holes that are also affected by airflow.

Fig. 1 shows the relationship between breathing and thermal changes over time. The yellow line represents one thermal image profile on the horizontal axis in the nose regions, and the black line represents the time axis (4 s). During inspiration, the temperature decreases as cold outside air is inhaled, and the temperature recovers during expiration. The red box shows the temperature changes over time in the nostril holes. The nostril hole is the passageway through which air is moved by breathing and is where the temperature changes with breathing are most dominant. The blue box shows the temperature changes over time the around the nostril holes. The region of the blue box is indirectly affected by the air being moved by breathing. The blue region shows relatively less change in temperature than the nostril hole, but it can be used as information to extract the breathing signals when the nostril hole is not well visible. The temperature changes caused by breathing around the nostril are difficult to define because the structure features change greatly depending on the individual size, location and measurement angle. Therefore, physiological features associated with breathing should be used to define the BAFRs.

B. BREATHING-ASSOCIATED PROBABILITY MAP (BAP)

The proposed algorithm used the time-varying change in temperature from breathing to estimate the association with breathing as a probability. The general breathing features can be represented as periodic signals with peaks and valleys due to temperature changes from breathing in thermal camera. In contrast, if the region is unassociated with breathing including apnea, the peak and valley characteristics decrease or disappear. In other words, the more the region is unassociated with breathing, the stronger the breathing-associated

features. Amplitude differences cause variance differences, which can be used to distinguish the differences in the influence of pixels associated with breathing. The proposed algorithm defines these features as Breathing-Associated Features (BAF). Since BAF does not reflect structural features, physiological features associated with breathing can be used to define regions. The non-structural features of the BAF make algorithm possible to define regions of periodic temperature change associated with breathing at multiple angles and unregistered views. In particular, since the proposed algorithm extracts periodic features of breathing using BAF, it can extract regions that are highly associated with breathing even when the nostril hole is not visible. Each point can be expressed as a variance, the strength of which is used to create a breathing-associated probability map. Fig. 2 shows the BAF, breathing-associated probability map and segmentation mask obtained using MRFs. The BAF is calculated with the following equation (1):

$$BAF\,(x, y, t) = \sqrt{\frac{1}{N_t - 1}\sum_{k=0}^{N_t-1}(BS\,[k] - \mu_{BS})^2} \qquad (1)$$

where x and y denote the coordinates of the ROI and t denotes the specific time on the time axis. N_t is the frame number corresponding to the observation time. In this study, the N_t corresponding to 4 s was used. The 4 s parameter is the average time for normal breathing. For fast breathing, the proposed algorithm can reflect the effect of breathing because there is a breathing signal within 4 s. For slow breathing, the algorithm includes a portion of the breathing signals, making it robust to a wide range of breathing rates. Increasing the N_t calculates the impact of breathing over a longer period. In addition, k is a natural number between 0 and N_t. Since the breathing signal shows time-related temperature changes caused by breathing, this signal can be calculated by cumulatively summing the change at each $k = 0$ frame point. μ_{BS} is the mean value of the BS. The breathing-associated probability (BAP) is calculated by dividing the calculated BAF by the maximum BAF value at the corresponding t. The BAP is calculated with Equation 2 as follows:

$$BAP\,(x, y, t) = \frac{1}{\arg\max(BAF\,(t))}BAF\,(x, y, t) \qquad (2)$$

C. EXPERIMENTAL SETTINGS

Thermal camera data and the reference signal were used to verify the breathing signals obtained by the proposed segmentation algorithm. The aspect of the BAFR projection varies depending on the angle at which the thermal camera data were acquired. Regions are directly or indirectly affected by temperature through the movement of breathing air during breathing, and depending on these properties, the temperature changes associated with breathing differ for each area. Generally, as the nostril area has a great influence on airflow during breathing, the temperature changes are the largest in this region, which is shown as a structural feature in the thermal face image. Experiments were conducted under various conditions to verify whether the proposed algorithm could extract physiological pixels.

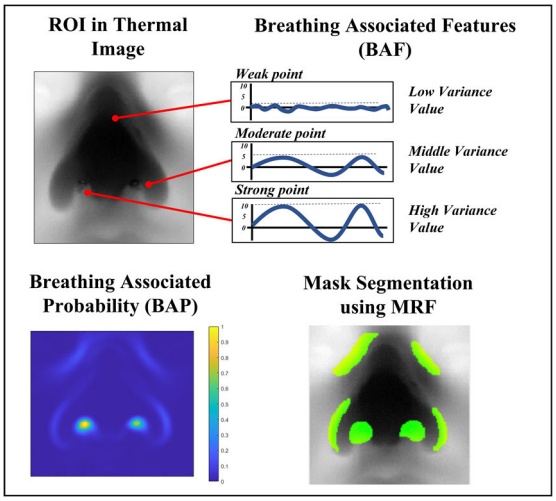

FIGURE 2. Concept of breathing-associated feature extraction and segmentation.

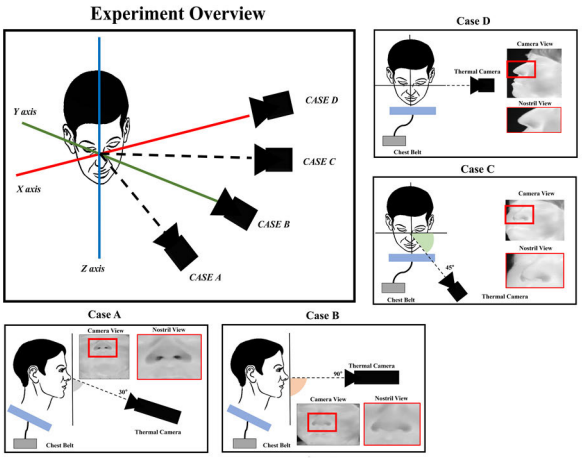

FIGURE 3. Experimental settings.

Fig. 3 shows the experimental settings. First, the best visible aspect of the nostril was determined at an angle of 30 degrees from the front (Case A). As the temperature change is largest in the nostril region, the structural features are clear in this area; thus, this view is typically used for breathing monitoring. Second, the invisible aspect of the nostril was determined at an angle of 90 degrees from the front (Case B). The thermal faces obtained at these angles do not contain stable nostrils. Third, the aspect was determined at an angle of 45 angles, not the front view (Case C). Finally, the aspect was determined at an angle of 90 angles, not the front view (Case D). The thermal faces acquired under the Case C and Case D conditions can include various BAFRs depending on the individual, which makes it difficult to define the region using structural information. 15 subjects participated in this study. The subjects consisted of healthy volunteers.

IEEE Journal of Translational Engineering in Health and Medicine

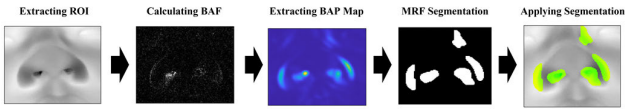

FIGURE 4. Processing flow chart.

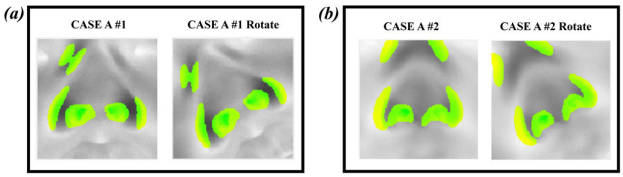

FIGURE 5. Representative results of the segmentation mask (Case A). (a) Example 1 of Case A. (b) Example 2 of Case A.

The subjects participated in the experiment after hearing sufficient explanations in the laboratory and providing consent. In addition, an anesthesiologist conducted an experiment to prevent problems caused by abnormal breathing. The present study was performed at Severance Hospital from July 2021 to August 2021. This study was conducted in accordance with the principles of Good Clinical Practice and was approved by the Institutional Research Board of Severance Hospital (Reference No. 4-2020-1320); all patients gave written informed consent. The study was registered at ClinicalTrails.Gov with the number NCT04964245. The distance between the subject and the thermal camera was 50 cm, and normal breathing was performed in a stable state. Five 1-minute measurements were taken for each subject. The thermal camera was the A655sc model (FLIR systems), and the camera data were acquired at 640 × 480 spatial resolution, 0.03 Kelvin temperature resolution, and 25 Hz. The breathing signal obtained by the chest belt sensor was used as a reference signal. A Biopac (MP150, Biopac Systems Inc) was used for reference measurements, and the chest belt sensor signal was measured at 1000 Hz.

D. PROCESSING

Through Kanade-Lucas-Tomasi (KLT) tracking, various ROIs in the nose were sorted in frame order [47]. In the first (Case A) and second (Case B) experiments, the ROIs were extracted simultaneously after rotation to determine the semantic segmentation properties of the proposed algorithm. Based on the obtained ROI, a BAP map was constructed by obtaining the BAF value in each pixel using a 4 s moving window. Figs. 4 show the processing flow charts.

The mask was extracted by applying MRF segmentation with the extracted BAP map. The class parameter of MRF was set to 2 to classify BAFR and non-BAFR. In addition, pixel clustering was performed by converging sufficiently through 30 iterations of each frame. All breathing signals were obtained by integrating the frame difference obtained from the differential temperature. To verify whether the proposed algorithm could extract the BAFR well, the breathing signals obtained with and without the application of the segmentation mask were compared.

III. RESULTS

The masks obtained in each experiment and the breathing signals obtained by applying the segmentation mask are shown in the figures below. The segmentation masks extracted by the proposed algorithm under various conditions were used to define the BAFR. Then, the breathing signals extracted by applying the defined segmentation mask and those extracted without the mask were compared. Among the two graphs for each sample, the upper and lower graphs represent the breathing signals obtained without and with segmentation mask application. In each graph, the blue signal represents the correct reference breathing signal obtained by the chest belt sensor, and the orange signal represents the noncontact breathing signal obtained by the thermal camera. The black region represents the thermal signal average trend. The overall results, the breathing signals obtained with the segmentation mask were extracted by removing unnecessary noise, which improved the breathing signal and allowed breathing to be recognized.

A. SEGMENTATION MASKS AND BREATHING SIGNALS OF CASE A

Fig. 5 shows the general segmentation masks for Case A. Fig. 5 (a) displays example 1 of Case A, and (b) displays example 2 of Case A. Each example includes an unregistered rotation situation. The ROI is expressed in grayscale, and the green color represents BAFR pixels. In the locations where the nostril is well observed (CASE A), the proposed segmentation algorithm extracted the BAFR well. Since the proposed algorithm performs pixel clustering based on the region with high breathing-associated probability within the ROI, the algorithm mainly extracted BAFRs in the nostril region. The proposed algorithm could extract the BAFR well even when the images were rotated. These results indicate that the proposed algorithm extracts semantic BAF well, which means that no additional image registration is required to estimate the breathing signals.

Fig. 6 shows a comparison between the breathing signals extracted by applying the segmentation mask and those obtained without applying the segmentation mask of Case A. Fig. 6 (a) shows example 1 of Case A, and (b) shows example 2 of Case A. In Case A, most of the breathing cycles were extracted to the extent that we could recognize breathing even when the mask was not applied. This result is due to the inclusion of the nostril holes, which changes temperature dominantly with breathing. However, there are cases in which the stability of the breathing signal is low even in the nostril holes. In these cases, noise is generated, and the breathing cycle is not recognized. Comparing the top orange signal(without the proposed algorithm) and the bottom orange signal(with the proposed algorithm) in Fig. 6 (a) and (b), The results show improved breathing signals.

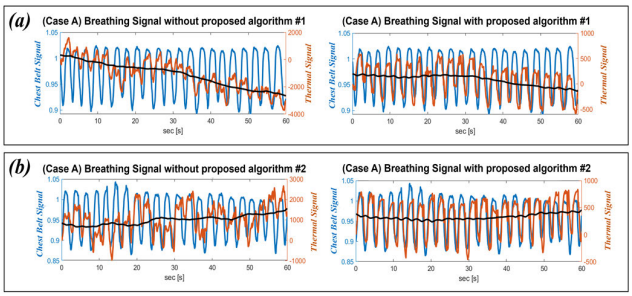

FIGURE 6. Representative results of the comparison between the breathing signals extracted with and without the application of a mask. (Case A). (a) Example 1 of Case A. (b) Example 2 of Case A.

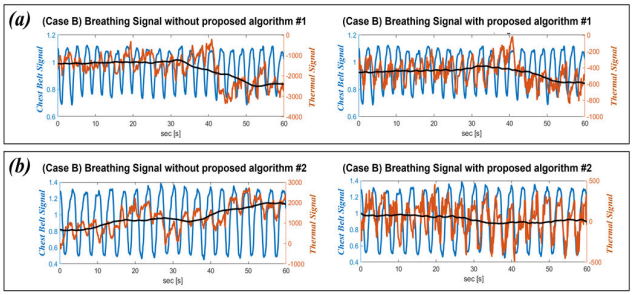

FIGURE 8. Representative results of the comparison between the breathing signals extracted with and without mask application. (Case B). (a) Example 1 of Case B. (b) Example 2 of Case B.

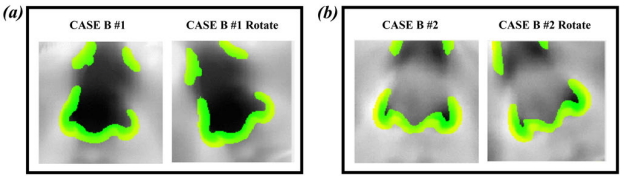

FIGURE 7. Representative results of the segmentation mask (Case B). (a) Example 1 of Case B. (b) Example 2 of Case B.

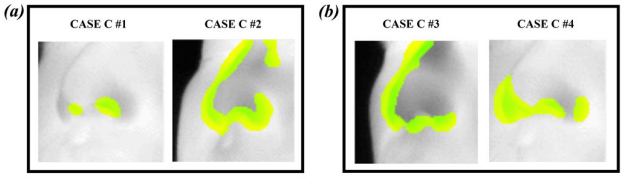

FIGURE 9. Representative results of the segmentation mask (Case C). (a) Examples 1 and 2 of Case C. (b) Examples 3 and 4 of Case C.

The breathing signals extracted by applying the proposed algorithm was stably improved.

B. SEGMENTATION MASKS AND BREATHING SIGNALS OF CASE B

Fig. 7 shows the segmentation masks for Case B. Fig. 7 (a) presents example 1 of Case B, and (b) presents example 2 of Case B. Each example includes an unregistered rotation situation too. Even in regions where nostril holes are not observed, the proposed algorithm extracted the BAFR well. Since the nostril was not included, the region around the nostril was defined as a BAFR by the proposed algorithm. The extracted regions were regions where air movement occurred due to periodic breathing and temperature changes. The extracted regions were defined around the nostril edge, which is the most affected part when airflow due to breathing occurs in the nostril direction. The proposed algorithm could extract BAFR even when the images were rotated too.

Fig. 8 shows a comparison between the breathing signals extracted by applying the segmentation mask and those obtained without applying the segmentation mask of Case B. Fig. 8 (a) shows example 1 of Case B, and (b) shows example 2 of Case B. When the nostril area was not visible, the breathing signal was unstable, which makes it difficult to analyze the breathing patterns. In a view that does not include nostril holes, the most dominant region of the temperature changes due to breathing is lost. Additionally, previous methods can not define BAFR using a nostril hole as a structural feature with dominant temperature variations. However, when the semantic segmentation mask was extracted with the proposed algorithm using physiological BAF, the breathing signals were improved, and the breathing cycle was recognized. Comparing the top orange signal (without the proposed algorithm) and the bottom orange signal(with the proposed algorithm) in Fig. 8 (a) and (b), The results show the restored breathing signals.

C. SEGMENTATION MASKS AND BREATHING SIGNALS OF CASE C

Fig. 9 shows the segmentation masks for Case C. Fig. 9 (a) illustrates examples 1 and 2 of Case C, and (b) illustrates examples 3 and 4 of Case C. In the location with a 45-degree angle, as opposed to the front view, the proposed segmentation algorithm extracted the BAFR well. Thermal facial data taken at 45 degrees include nostril holes in some samples and not in others. This is individual characteristic that varies depending on the position of the nostril holes, the shape of the nose, etc. Also, As the angle changes from the front view, more regions that are not associated with breathing are included in the thermal projection. Similar to Case B, in view where the nostril hole is not represented, it is difficult to apply previous algorithms that utilize the nostril hole as a structural feature to extract BAFR. Despite these conditions, the proposed algorithm robustly extracted BAFR. In subjects with visible nostril holes, BAFR was extracted around the nostril holes. And in subjects without visible nostril holes, BAFR was extracted in the high associated breathing region of the acquired frame. These results show that the proposed algorithm can be helpful for the robust and stable extraction of breathing signals in various clinical environments. Thus, the proposed algorithm is important for practical breathing monitoring.

Fig. 10 shows a comparison between the breathing signals extracted by applying the segmentation mask and those

IEEE Journal of Translational Engineering in Health and Medicine

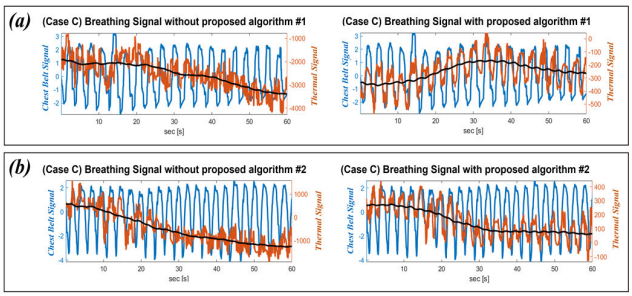

FIGURE 10. Representative results of the comparison between the breathing signals extracted with and without mask application. (Case C). (a) Example 1 of Case C. (b) Example 2 of Case C.

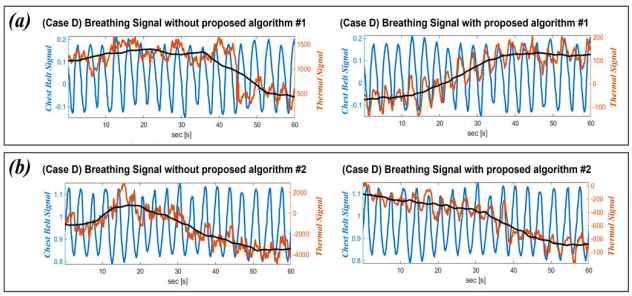

FIGURE 12. Representative results of the comparison between the breathing signals extracted with and without mask application. (Case D). (a) Example 1 of Case D. (b) Example 2 of Case D.

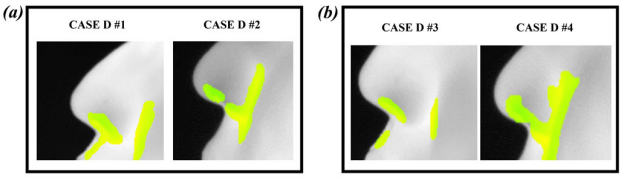

FIGURE 11. Representative results of the segmentation mask (Case D). (a) Examples 1 and 2 of Case D. (b) Examples 3 and 4 of Case D.

obtained without applying the segmentation mask. Fig. 10 (a) shows example 1 of Case C, and (b) shows example 2 of Case C. At an angle other than the front view, it is difficult to extract a breathing signal without defining a BAFR. It is difficult to extract breathing signals from non-frontal views. Because the previous algorithm using structured features is difficult to apply. As the view changes, the information in regions associated with breathing is lost and regions not associated with breathing are increased. When the proposed algorithm is applied, stable breathing signals can be extracted, thereby allowing breathing monitoring, even at 45 degrees. The proposed algorithm uses physiological BAF to extract the regions associated with breathing at a given frame, making it view-independent. Comparing the top orange signal(without the proposed algorithm) and the bottom orange signal(with the proposed algorithm) in Fig. 10 (a) and (b), The results show the restored breathing signals.

D. SEGMENTATION MASKS AND BREATHING SIGNALS OF CASE D

Fig. 11 shows the segmentation masks for Case D. Fig. 11 (a) displays examples 1 and 2 of Case D, and (b) displays examples 3 and 4 of Case D. In the location at a 90-degree angle, as opposed to the front view, the proposed segmentation algorithm extracts the BAFR well too.

Fig. 12 shows a comparison between the breathing signals extracted by applying the segmentation mask and those obtained without applying the segmentation mask. Fig. 12 (a) presents example 1 of Case D, and (b) presents example 2 of Case D. When the breathing signals are extracted at various angles, more regions that are not associated with breathing are included than when the signals are extracted from the front view. The regions associated with breathing and the nostril are obscured and observed asymmetrically depending on the angle. Generally, when breathing signals are extracted at various angles and views, the breathing cycle cannot be recognized. In Case D, the region typically associated with breathing is low. Breathing signals were not extracted unless the BAFR is extracted. However, an improved breathing signal was extracted when the proposed algorithm was applied. Comparing the top orange signal(without the proposed algorithm) and the bottom orange signal(with the proposed algorithm) in Fig. 12 (a) and (b), The results show the restored breathing signals.

E. STATISTICAL RESULTS OF THE PROPOSED ALGORITHM

The statistical results of the proposed algorithm are presented as follows. We compared the number of breaths in the non-contact breathing signal obtained from the thermal camera with the reference obtained from the chest belt sensors. When the proposed algorithm was not used, the average accuracy was 65.6%; however, when the proposed algorithm was applied, the accuracy was improved to 90.9%. In addition, the average correlation value increased from 0.587 to 0.885. In Cases C and D, the accuracy and correlation were significantly improved. The accuracy of Case C increased by 31.5%, from 56.9% to 88.4%, and the accuracy of Case D increased by 35.9% from 49.8% to 85.7%. The correlation of Case C increased by 0.205, from 0.689 to 0.894, and the correlation of Case D increased by 0.258, from 0.589 to 0.847. The reason is that Cases C and D have more regions that are not associated with breathing than Cases A and B, so the proposed algorithm effectively removes noise. Table 1 shows the number of breathing cycles and accuracy for each case.

The comparison with previous methods, measured in a stable environment with visible nostrils using a thermal imaging camera, is shown in Table 2. In this study, the comparable environment to the existing method is Case A. The proposed algorithm achieved 99.0% accuracy in Case A, where the nostril is well visible, outperforming, or equal to other methods. The proposed algorithm is not only able to extract stable breathing signals in the nostril visible (Case A), but also

TABLE 1. The number of breathing cycles and statistical results.

Case	Reference (chest)	Without Mask (accuracy)	With Mask (accuracy)	Average Breathing Rate (1min)	Correlation (without/ with)
Case A	1,328	1,188 (89.4%)	1,315 (99.0%)	17.70	(0.961/ 0.985)
Case B	1,338	899 (64.7%)	1,245 (89.7%)	18.80	(0.762/ 0.914)
Case C	1,292	738 (57.1%)	1,146 (88.6%)	17.22	(0.689/ 0.894)
Case D	1,210	601 (49.6%)	1,040 (85.9%)	16.13	(0.589/ 0.847)
Total	5,218	3,426 (65.6%)	4,746 (90.9%)	17.39	(0.587/ 0.885)

TABLE 2. comparison accuracy of previous methods.

Method	Accuracy
A. Basu [36]	91.3 %
Abbas [32]	97.7 %
Rumiński [33]	97.6 %
A. H. Alkali [37]	98.2 %
J. Fei [28]	98.3 %
Shu [34]	98.8 %
Ours (Case A)	99.0 %

in the invisible aspect of the nostril was determined at an angle of 90 degrees from the front (Case B), the aspect was determined at an angle of 45 angles, not the front view (Case C), and the aspect was determined at an angle of 90 angles, not the front view (Case D). By extracting physiological breathing-associated features from thermal cameras, the proposed algorithm was able to extract stable breathing signals from various angles that the previous methods face challenges while maintaining the advantages of the previous methods.

IV. DISCUSSION

Measuring noncontact breathing signals is important for monitoring clinical conditions. Breathing is a critical part of life and should be monitored continuously and reliably in various clinical environments. Contact methods are limited by infection risks and inconvenience. To offset the disadvantage of contact methods, non-contact methods of measuring breathing have been developed, including RGB, Depth, Rader, and Thermal camera methods. In particular, it has been shown that thermal cameras can be used in the absence of light and can be used to measure the volume of breathing [42]. However, Thermal cameras cannot directly measure structural information, and there is a relative loss of structural information when using an RGB depth camera. Thus, due to the characteristics of thermal cameras, BAFR segmentation using structural methods has limited meaning and performance. Moreover, the previous method using the structural features is difficult to apply at various views, and the performance is highly variable depending on the inclusion of the nostril holes.

In this study, we propose a semantic segmentation method that reflects temperature changes due to actual breathing. The proposed algorithm uses physiological BAF to extract the BAFR at various angles and views. Each pixel is labeled as a BAFR or non-BAFR using MRF. The proposed segmentation algorithm can identify stable and reliable breathing signals. The results show that the breathing signals can be extracted at various angles and views. Even if the thermal camera is operated under various conditions, the breathing characteristics are reflected as 2D projections. The algorithm extracts breathing characteristics according to the projected temperature and defines regions associated with breathing. As the proposed algorithm labels each pixel and uses BAF, even if the angle of the thermal projection changes, the algorithm can extract the adaptive BAFR. These properties can be helpful when breathing should be measured efficiently in various clinical environments. Figs. 5, 7, 9, and 11 show the BAFRs obtained using the proposed algorithm at various aspects and views. Since the region projected by the thermal camera differs, the 2D regions of the extracted BAFR vary. However, when the results are comprehensively judged in three dimensions, the extracted BAFRs show structurally similar regions. Based on the extracted BAFRs, we can identify the structural regions that are most associated with breathing. In terms of statistics, the average accuracy was 65.6% without the algorithm, but it increased to 90.9% when the algorithm was applied. The average correlation value also rose from 0.587 to 0.885. Notably, Cases C and D saw significant enhancements in both accuracy and correlation due to having more non-breathing associated regions, which the algorithm effectively filtered out. Case C's accuracy increased from 57.1% to 88.7% and correlation from 0.689 to 0.894. Case D's accuracy rose from 49.6% to 85.9%, with the correlation moving from 0.589 to 0.847. In previous works, breathing was simply measured by estimating regions that were likely to be associated with breathing. However, the proposed algorithm can visualize regions associated with breathing based on the periodicity of breathing. The proposed algorithm consistently captures breathing signals not only from a frontal, visible nostril perspective (Case A) but also from less accessible views: at a 90-degree angle from the front with an obscured nostril (Case B), at a non-frontal 45-degree angle (Case C), and at a non-frontal 90-degree angle (Case D). By utilizing thermal cameras to extract physiological features associated with breathing, the algorithm successfully derives stable breathing signals from angles traditionally challenging for existing methodologies, all the while retaining their beneficial aspects. In other words, the proposed algorithm provides a method to observe the shape of the region associated with breathing. Furthermore, it is significant that the proposed algorithm provides a basic approach for observing changes in the BAFR depending on the type of breathing, which can be applied to investigate clinical diseases with nasal obstruction.

In this study, Experiments were conducted to verify the feasibility of the proposed algorithm in a stable state. To use the algorithm in practical settings, experiments should be conducted at more specified subjects' cases, diverse angles, and in various environments. Additionally, the

IEEE Journal of Translational Engineering in Health and Medicine

real-time application is difficult because computing resources are greatly consumed using ICM. However, the proposed algorithm is a potential method for extracting physiological features that overcome the limitations of existing structural feature methods.

Measuring breathing with thermal cameras can overcome the drawbacks of existing contact methods. However, due to the nature of noncontact methods, noncontact methods require more stable environments than contact methods. These unstable characteristics lead to difficulties in the practical use of noncontact methods using thermal cameras. In a realistic clinical environment, the patient and the thermal camera are not looking perfectly straight ahead, and the shape and position of the nostril are not measured under optimal circumstances. The proposed algorithm can be utilized as a method to extract robust breathing signals in various practice environments for reliable breathing monitoring while maintaining the advantages of previous methods. The proposed algorithm could extract breathing signals not only from the front view of the face but also from various aspects and angles, thereby improving the feasibility of breathing monitoring with thermal cameras in clinical environments such as an isolated ward, operation rooms, and ICUs where infection risks are high. Overall, the use of thermal cameras for non-contact breathing monitoring using proposed algorithm has the potential to improve clinical practice and patient outcomes. The proposed algorithm can help transform breathing monitoring technology using thermal cameras into innovative and functional products.

V. CONCLUSION

In this study, we propose a semantic segmentation method that takes into account temperature changes in breathing. The proposed algorithm utilizes physiological BAF to extract BAFR from various angles and views. When the proposed algorithm was not used, the average accuracy was 65.6%; however, when the proposed algorithm was applied, the accuracy was improved to 90.7%. The average correlation value also increases from 0.587 to 0.885. The results showed that when the proposed algorithm was applied, the accuracy of segmentation was significantly improved, especially in 45-degree and 90-degree views. The algorithm was also able to accurately extract BAFR from the nose region, regardless of the angle, and segment more precise regions at the pixel level in the thermal camera. The proposed segmentation algorithm can extract stable breathing signals and accurately identify breathing cycles.

REFERENCES

[1] S. R. Braun, "Respiratory rate and pattern," in *Clinical Methods: The History, Physical, and Laboratory Examinations*, H. Walker, W. Hall, and J. Hurst, Eds. Boston, MA, USA: Butterworths, 1990, pp. 226–230.

[2] M. J. Tobin, "Respiratory monitoring in the intensive care unit," *Amer. Rev. Respiratory Disease*, vol. 138, no. 6, pp. 1625–1642, Dec. 1988, doi: 10.1164/ajrccm/138.6.1625.

[3] J. D. Truwit and D. F. Rochester, "Monitoring the respiratory system of the mechanically ventilated patient," *New Horiz.*, vol. 2, no. 1, pp. 94–106, Feb. 1994.

[4] M. A. Cretikos, R. Bellomo, K. Hillman, J. Chen, S. Finfer, and A. Flabouris, "Respiratory rate: The neglected vital sign," *Med. J. Aust.*, vol. 188, no. 11, pp. 657–659, Jun. 2008, doi: 10.5694/j.1326-5377.2008.tb01825.x.

[5] M. M. Churpek, T. C. Yuen, S. Y. Park, D. O. Meltzer, J. B. Hall, and D. P. Edelson, "Derivation of a cardiac arrest prediction model using ward vital signs," *Crit. Care Med.*, vol. 40, no. 7, pp. 2102–2108, Jul. 2012, doi: 10.1097/CCM.0b013e318250aa5a.

[6] I. Homma and Y. Masaoka, "Breathing rhythms and emotions," *Exp. Physiol.*, vol. 93, no. 9, pp. 1011–1021, Aug. 2008, doi: 10.1113/expphysiol.2008.042424.

[7] M. Grassmann, E. Vlemincx, A. von Leupoldt, J. M. Mittelstädt, and O. Van den Bergh, "Respiratory changes in response to cognitive load: A systematic review," *Neural Plasticity*, vol. 2016, Jun. 2016, Art. no. 8146809, doi: 10.1155/2016/8146809.

[8] D. Goodman et al., "Challenges in the diagnosis of paediatric pneumonia in intervention field trials: Recommendations from a pneumonia field trial working group," *Lancet Respiratory Med.*, vol. 7, no. 12, pp. 1068–1083, Dec. 2019, doi: 10.1016/S2213-2600(19)30249-8.

[9] J. Lee and S. K. Yoo, "Respiration rate estimation based on independent component analysis of accelerometer data: Pilot single-arm intervention study," *JMIR mHealth uHealth*, vol. 8, no. 8, Aug. 2020, Art. no. e17803, doi: 10.2196/17803.

[10] P. H. Quanjer, G. J. Tammeling, J. E. Cotes, O. F. Pedersen, R. Peslin, and J.-C. Yernault, "Lung volumes and forced ventilatory flows," *Eur. Respiratory J.*, vol. 6, no. 16, pp. 5–40, Mar. 1993, doi: 10.1183/09041950.005s1693.

[11] A. J. Lopes, "Advances in spirometry testing for lung function analysis," *Expert Rev. Respiratory Med.*, vol. 13, no. 6, pp. 559–569, Jun. 2019, doi: 10.1080/17476348.2019.1607301.

[12] J. W. Kreit, "Volume capnography in the intensive care unit: Physiological principles, measurements, and calculations," *Ann. Amer. Thoracic Soc.*, vol. 3, pp. 291–300, Mar. 2019, doi: 10.1513/AnnalsATS.201807-501CME.

[13] R. G. Soto, E. S. Fu, H. Vila, and R. V. Miguel, "Capnography accurately detects apnea during monitored anesthesia care," *Anesthesia Analgesia*, vol. 99, no. 2, pp. 379–382, Aug. 2004, doi: 10.1213/01.ANE.0000131964.67524.E7.

[14] A. S. Khalafalla, S. P. Stackhouse, and O. H. Schmitt, "Thoracic impedance gradient with respect to breathing," *IEEE Trans. Biomed. Eng.*, vols. BME-17, no. 3, pp. 191–198, Jul. 1970, doi: 10.1109/TBME.1970.4502733.

[15] J. H. Houtveen, P. F. C. Groot, and E. J. C. de Geus, "Validation of the thoracic impedance derived respiratory signal using multilevel analysis," *Int. J. Psychophysiology*, vol. 59, no. 2, pp. 97–106, Feb. 2006, doi: 10.1016/j.ijpsycho.2005.02.003.

[16] L. Guan et al., "Multi-person breathing detection with switching antenna array based on WiFi signal," *IEEE J. Transl. Eng. Health Med.*, vol. 11, pp. 23–31, 2023, doi: 10.1109/JTEHM.2022.3218638.

[17] C. Romano, E. Schena, S. Silvestri, and C. Massaroni, "Non-contact respiratory monitoring using an RGB camera for real-world applications," *Sensors*, vol. 21, no. 15, p. 5126, Jul. 2021, doi: 10.3390/s21155126.

[18] C. Massaroni, D. Lo Presti, D. Formica, S. Silvestri, and E. Schena, "Non-contact monitoring of breathing pattern and respiratory rate via RGB signal measurement," *Sensors*, vol. 19, no. 12, p. 2758, Jun. 2019, doi: 10.3390/s19122758.

[19] H. Wang and S. Zhang, "Non-contact human respiratory rate measurement under dark environments by low-light video enhancement," *Biomed. Signal Process. Control*, vol. 85, Aug. 2023, Art. no. 104874, doi: 10.1016/j.bspc.2023.104874.

[20] E. P. Doheny et al., "Estimation of respiratory rate and exhale duration using audio signals recorded by smartphone microphones," *Biomed. Signal Process. Control*, vol. 80, Feb. 2023, Art. no. 104318, doi: 10.1016/j.bspc.2022.104318.

[21] Y. S. Lee, P. N. Pathirana, T. Caelli, and R. Evans, "Doppler radar in respiratory monitoring: Detection and analysis," in *Proc. Int. Conf. Control, Autom. Inf. Sci. (ICCAIS)*, Nov. 2013, pp. 224–228.

[22] J. Lee and S. K. Yoo, "Radar-based detection of respiration rate with adaptive harmonic quefrency selection," *Sensors*, vol. 20, no. 6, p. 1607, Mar. 2020, doi: 10.3390/s20061607.

[23] K. Oh, C. S. Shin, J. Kim, and S. K. Yoo, "Level-set segmentation-based respiratory volume estimation using a depth camera," *IEEE J. Biomed. Health Informat.*, vol. 23, no. 4, pp. 1674–1682, Jul. 2019, doi: 10.1109/JBHI.2018.2870859.

[24] Y. Shan, S. Li, and T. Chen, "Respiratory signal and human stress: Non-contact detection of stress with a low-cost depth sensing camera," *Int. J. Mach. Learn. Cybern.*, vol. 11, no. 8, pp. 1825–1837, Feb. 2020, doi: 10.1007/s13042-020-01074-x.

[25] J. Kwon, O. Kwon, K. Oh, J. Kim, C. S. Shin, and S. K. Yoo, "Thermodiluted relative tidal volume estimation using a thermal camera in operating room under spinal anesthesia," *Biomed. Eng. OnLine*, vol. 21, no. 1, p. 64, Sep. 2022, doi: 10.1186/s12938-022-01028-0.

[26] Y. Takahashi, Y. Gu, T. Nakada, R. Abe, and T. Nakaguchi, "Estimation of respiratory rate from thermography using respiratory likelihood index," *Sensors*, vol. 21, no. 13, p. 4406, Jun. 2021, doi: 10.3390/s21134406.

[27] J. Fei and I. Pavlidis, "Virtual thermistor," in *Proc. 29th Annu. Int. Conf. IEEE Eng. Med. Biol. Soc.*, Lyon, Aug. 2007, pp. 250–253.

[28] J. Fei and I. Pavlidis, "Thermistor at a distance: Unobtrusive measurement of breathing," *IEEE Trans. Biomed. Eng.*, vol. 57, no. 4, pp. 988–998, Apr. 2010, doi: 10.1109/TBME.2009.2032415.

[29] C. B. Pereira, X. Yu, V. Blazek, and S. Leonhardt, "Robust remote monitoring of breathing function by using infrared thermography," in *Proc. 37th Annu. Int. Conf. IEEE Eng. Med. Biol. Soc. (EMBC)*, Milan, Italy, Aug. 2015, pp. 4250–4253.

[30] C. B. Pereira et al., "Noncontact monitoring of respiratory rate in newborn infants using thermal imaging," *IEEE Trans. Biomed. Eng.*, vol. 66, no. 4, pp. 1105–1114, Apr. 2019, doi: 10.1109/TBME.2018.2866878.

[31] I. Lorato et al., "Automatic separation of respiratory flow from motion in thermal videos for infant apnea detection," *Sensors*, vol. 21, no. 18, p. 6306, Sep. 2021, doi: 10.3390/s21186306.

[32] A. K. Abbas, K. Heimann, K. Jergus, T. Orlikowsky, and S. Leonhardt, "Neonatal non-contact respiratory monitoring based on real-time infrared thermography," *Biomed. Eng. OnLine*, vol. 10, no. 1, p. 93, 2011, doi: 10.1186/1475-925X-10-93.

[33] J. Rumiński, "Evaluation of respiration rate and pattern using a portable thermal camera," in *Proc. Int. Conf. Quant. Infr. Thermography*, 2016, pp. 678–683, doi: 10.21611/qirt.2016.107.

[34] S. Shu, H. Liang, Y. Zhang, Y. Zhang, and Z. Yang, "Non-contact measurement of human respiration using an infrared thermal camera and the deep learning method," *Meas. Sci. Technol.*, vol. 33, no. 7, Apr. 2022, Art. no. 075202, doi: 10.1088/1361-6501/ac5ed9.

[35] G. C. Holst, "Spectral Dependence," in *Common Sense Approach to Thermal Imaging*. Washington, DC, USA: SPIE, 2000.

[36] A. Basu, A. Dasgupta, and A. Routray, "A thermographic method for detecting respiratory alkalosis by monitoring breath patterns," in *Proc. Int. Conf. Syst. Med. Biol. (ICSMB)*, Kharagpur, India, Jan. 2016, pp. 26–30.

[37] A. H. Alkali, R. Saatchi, H. Elphick, and D. Burke, "Thermal image processing for real-time non-contact respiration rate monitoring," *IET Circuits, Devices Syst.*, vol. 11, no. 2, pp. 142–148, Mar. 2017, doi: 10.1049/iet-cds.2016.0143.

[38] L. Maurya, P. Mahapatra, and D. Chawla, "Non-contact breathing monitoring by integrating RGB and thermal imaging via RGB-thermal image registration," *Biocybern. Biomed. Eng.*, vol. 41, no. 3, pp. 1107–1122, Jul. 2021, doi: 10.1016/j.bbe.2021.07.002.

[39] T. Zhang, Y. Xia, and D. D. Feng, "Hidden Markov random field model based brain MR image segmentation using clonal selection algorithm and Markov chain Monte Carlo method," *Biomed. Signal Process. Control*, vol. 12, pp. 10–18, Jul. 2014, doi: 10.1016/j.bspc.2013.07.010.

[40] K. Kayabol, E. E. Kuruoglu, and B. Sankur, "Bayesian separation of images modeled with MRFs using MCMC," *IEEE Trans. Image Process.*, vol. 18, no. 5, pp. 982–994, May 2009, doi: 10.1109/TIP.2009.2012905.

[41] J. Nie et al., "Automated brain tumor segmentation using spatial accuracy-weighted hidden Markov random field," *Computerized Med. Imag. Graph.*, vol. 33, no. 6, pp. 431–441, Sep. 2009, doi: 10.1016/j.compmedimag.2009.04.006.

[42] F. Destrempes, M. Mignotte, and J.-F. Angers, "A stochastic method for Bayesian estimation of hidden Markov random field models with application to a color model," *IEEE Trans. Image Process.*, vol. 14, no. 8, pp. 1096–1108, Aug. 2005, doi: 10.1109/tip.2005.851710.

[43] E. R. McFadden et al., "Thermal mapping of the airways in humans," *J. Appl. Physiol.*, vol. 58, no. 2, pp. 564–570, Feb. 1985, doi: 10.1152/jappl.1985.58.2.564.

[44] W. E. Holden, J. P. Wilkins, M. Harris, H. A. Milczuk, and G. D. Giraud, "Temperature conditioning of nasal air: Effects of vasoactive agents and involvement of nitric oxide," *J. Appl. Physiol.*, vol. 87, no. 4, pp. 1260–1265, Oct. 1999, doi: 10.1152/jappl.1999.87.4.1260.

[45] M. K. Marks, M. South, and B. G. Carter, "Measurement of respiratory rate and timing using a nasal thermocouple," *J. Clin. Monitor.*, vol. 11, no. 3, pp. 159–164, May 1995, doi: 10.1007/bf01617716.

[46] C. Massaroni, A. Nicolò, D. Lo Presti, M. Sacchetti, S. Silvestri, and E. Schena, "Contact-based methods for measuring respiratory rate," *Sensors*, vol. 19, no. 4, p. 908, Feb. 2019, doi: 10.3390/s19040908.

[47] S. Baker and I. Matthews, "Lucas-Kanade 20 years on: A unifying framework," *Int. J. Comput. Vis.*, vol. 56, no. 3, pp. 221–255, Feb. 2004, doi: 10.1023/b:visi.0000011205.11775.fd.